IEEE Photonics Journal
An IEEE Photonics Society Publication

Open Access

Lensless Miniature Portable Fluorometer for Measurement of Chlorophyll and CDOM in Water Using Fluorescence Contact Imaging

Volume 6, Number 3, June 2014

Lior Blockstein
Orly Yadid-Pecht, Fellow, IEEE

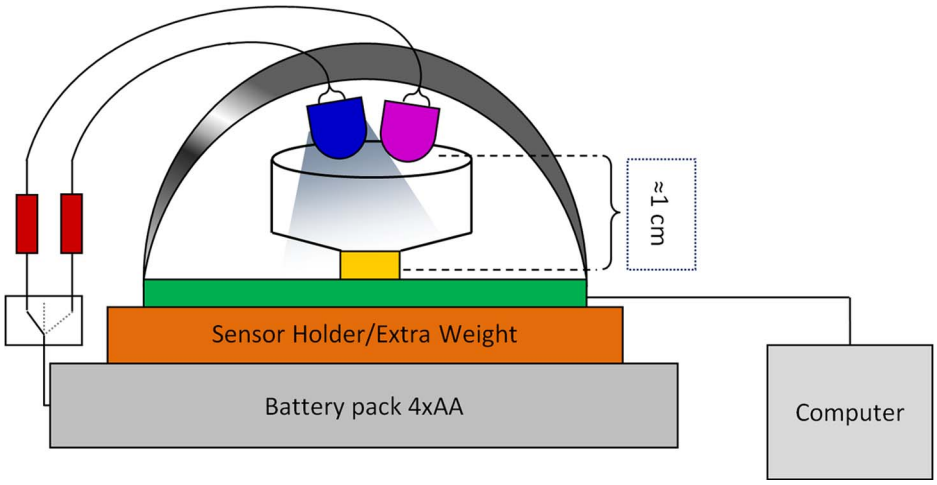

DOI: 10.1109/JPHOT.2014.2326665
1943-0655 © 2014 IEEE

IEEE photonics SOCIETY

IEEE

Lensless Miniature Portable Fluorometer for Measurement of Chlorophyll and CDOM in Water Using Fluorescence Contact Imaging

Lior Blockstein and Orly Yadid-Pecht, *Fellow, IEEE*

Department of Electrical and Computer Engineering, University of Calgary, Calgary, AB T2N 1N4, Canada

DOI: 10.1109/JPHOT.2014.2326665

Manuscript received April 2, 2014; revised May 9, 2014; accepted May 14, 2014. Date of publication June 2, 2014; date of current version June 12, 2014. The work of L. Blockstein was supported by NSERC. The work of O. Yadid-Pecht was supported by iCORE/AITF. Corresponding author: L. Blockstein (e-mail: blockstein@gmail.com).

Abstract: We report on the design, fabrication, and verification of a proof-of-concept miniature fluorometer, which is designed to measure chlorophyll and colored dissolved organic matter (CDOM) concentration in aquatic environment. The system utilizes light emitting diodes (LEDs) for fluorescence excitation and absorption filters for excitation light attenuation. The excitation LED for chlorophyll has peak emission at 465 nm, and the excitation LED for CDOM has peak emission at 341 nm. Our device demonstrates the concept of attaching two different absorption filters on a single sensor array for measuring the fluorescence signal from two different fluorescent dyes. We have tested the system's ability to detect fluorescence from various concentrations of fluorescein as a close simulant and the calibration standard for chlorophyll, and quinine sulfate dihydrate (QSD) as a simulant and calibration standard for CDOM. We have successfully acquired the fluorescent signal for fluorescein between 0.7 and 1000 nM and for QSD between 2.6 and 638 nM.

Index Terms: Contact imaging, lensless system, lensfree system, fluorescence, fluorescein, quinine sulfate dihydrate, CDOM, chlorophyll, fluorescent contact imaging.

1. Introduction

Water quality monitoring is a wide field of study with many applications. Water quality monitoring is necessary in aquaculture, desalination plants, hydraulic fracturing, source water, drinking water and wastewater. Additionally water monitoring of ocean water, coastal water, groundwater and surface water is performed for research and water quality monitoring.

Within these various applications monitoring water quality of surface water is one of the most important applications, due to its many uses. Surface water is located above the earth's surface and includes sources such as rivers, lakes, streams, ponds, water reservoirs, wetland, and others. Surface water provides a water source for aquatic life, wildlife and humans. Surface water uses include, but are not limited to public water supply, wild fish habitats, wild shellfish habitat, wild animal water supply, recreational activities, agricultural purposes and industrial uses. The effect of polluted surface water not only affects the aquatic life within the body of water, but it reaches out to all bio-life that feeds from that water source affecting the whole local ecosystem. Continuous monitoring (in contrast to casual monitoring) of surface water is imperative for continuous assessment of its ecological health, as well as anticipation and possible prevention of harmful phenomena

such as hypertrophication (algal bloom), hypoxia (low dissolved oxygen) and sediment plumes. However, monitoring water quality of surface water is a challenging task because of the continuous need for measurements and because of the wide spread and remote locations of many sources of surface water.

In this paper, we have chosen to concentrate on two key parameters observed in monitoring surface water quality; chlorophyll and colored dissolved organic material (CDOM). Chlorophyll is located in many living organisms such as plants, bacteria, algae and other phytoplankton. Chlorophyll is an essential component in the molecular photosynthesis mechanism and in turn, photosynthesis is an essential process, using the sunlight energy to produce oxygen, which is necessary to sustain life. Chlorophyll *a* is the most common type of chlorophyll. Other types of chlorophylls named *b*, *c*, *d* and *f* [1], [2] also contribute to the photosynthesis process and can be present within photosynthetic organisms previously mentioned. When measuring chlorophyll levels in water, chlorophyll *a* is usually measured because it is the dominant type of chlorophyll.

Measuring chlorophyll in water is a surrogate for measuring concentration of algae. Monitoring the algae population and its distribution is used to draw conclusions regarding the health of a body of water and the amount of food available to fuel its food chain. For example, small levels of algae will lead to a deficit and will not be enough to sustain a large biological community, while high levels of algae indicates that the amount of nutrients in the body of water is too high. This can also lead to a problem as, abundant algae will sink to the bottom and decay. The decay process will increase the levels of aerobic bacteria. Since aerobic bacteria use oxygen for metabolism, in large quantities, the bacteria will deplete the oxygen levels in the body of water.

Dissolved organic matter (DOM) is one of the largest reservoirs of organic carbon in water [3]–[5]. CDOM is the colored component of DOM, and can be optically measured. Several published studies have shown that there is a strong correlation between CDOM to DOM [6]–[8]. Hence, measuring the CDOM component is a non-direct measurement of DOM. DOM fuels the microbial loop by fueling bacterial respiration because it carries a large amount of carbon, nitrogen and phosphorus. Therefore, an abundance of DOM contributes to eutrophication. CDOM has high absorbance in the UV range and the blue range; this allows CDOM to protect the aquatic life from harmful UV radiation, an effect that is more important for high-latitude bodies of water [9], [10].

Both chlorophyll *a* and CDOM are fluorescent, a property that can be employed to measure their concentration in water. Fluorescent molecules are able to absorb excitation light and re-emit emission light at longer wavelength. The emission light is usually significantly, weaker due to small concentration of the fluorophores or small sample size. The concentration of CDOM or chlorophyll-*a* in water can be as low as 0.1 nM. Due to the very low concentration the fluorescent signal can be 10^{-4} to 10^{-6} [16], [17] times less than the excitation signal.

Portable devices utilize the fluorescent property of molecules to determine the concentration of the fluorescent matter in water. Recent studies have demonstrated miniature, portable and low power devices for the measuring of chlorophyll *a* in aquatic environment [11], [18]–[20]. However, much less has been done for CDOM. While the majority of the commercially available devices measure a single parameter [21], the few commercial devices that do offer multi-sensor platform for measurement of both chlorophyll *a* and CDOM concentration in water are expensive (over $8000). In this paper, we report a compact, low power, low cost multi-sensor prototype for measuring chlorophyll *a* and CDOM under water by using contact fluorescent imaging.

Contact fluorescent imaging is a recently developed method of micro imaging where the fluorescent sample of interest is coupled to the emission filter which overlays the sensor array. The image is acquired by projecting excitation light on the coupled sample and capturing the emission light emitted by the sample. This approach eliminates the need for conventional optical components. While conventional imaging continues to provide better spatial resolution, contact imaging offers other advantages such as better light collection efficiency [22]–[24] lower cost, reduced weight and size, low power requirements and portability.

In this current study, a Polyvinyl acetate (PVAc) [15] Bismarck brown Y (PVAcBBY) and Polyvinyl acetate Benzophenone-8 (PVAcB-8) filter was manufactured on top of ultra-thin glass ribbon (UTGR) and attached to a sensor array of a CMOS image sensor (CIS). In addition to its simple

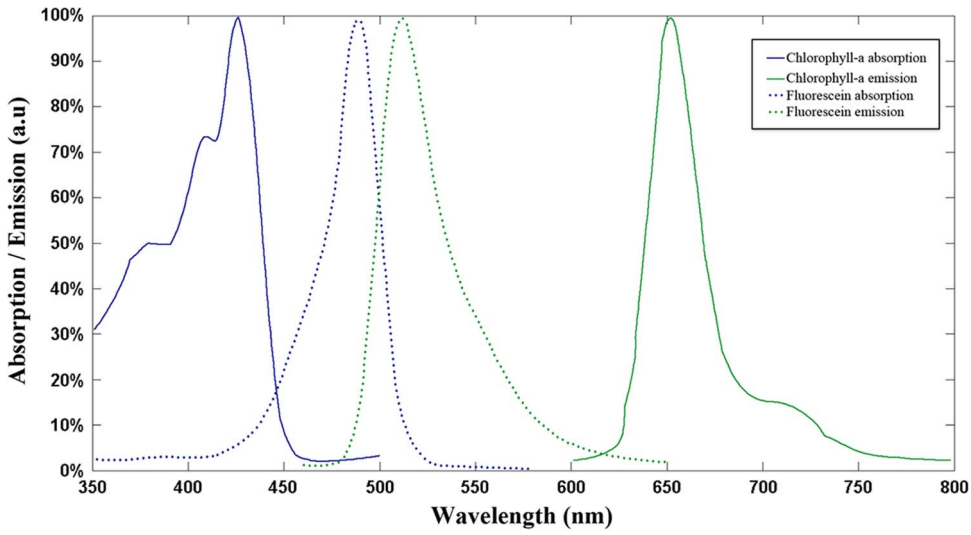

Fig. 1. Absorption and emission spectrum of chlorophyll *a* and fluorescein. Fluorescein is often used as a simulant for chlorophyll *a*, and it is a fluorescent standard for instrument performance checks and calibration of chlorophyll *a* fluorometers.

design and fabrication process, the filter can also be easily removed from the sensor, allowing reusability of the sensors.

In this manuscript, Section 2 describes the method used to select the excitation light and emission filter for chlorophyll *a* measurement, Section 3 shortly reviews the excitation light and the emission filter used by the system for CDOM measurement, Section 4 describes the integration of all the selected components to create a lensless miniature portable fluorometer for measurement of chlorophyll *a* and CDOM in water, Section 5 reports how the fluorometer was calibrated using quinine sulfate dihydrate and fluorescein, Section 5 also benchmarks the system in comparison with other similar systems. Section 6 summarizes the conclusions.

2. Excitation Source and Emission Filter for Lensless Miniature Portable Fluorometer for Measurement of Chlorophyll in Water

When exposed to excitation light (peak at 430 nm), chlorophyll *a* is unstable. It is quickly converted to several byproducts, with the main ones being chlorophyll *b* and pheophytin [25]–[27]. This adds an unknown variable to fluorescence measurements, to avoid this Kissinger *et al.* [18] used fluorescein sodium salt (FSS) as a chlorophyll *a* simulant in their lifetime detection fluorometer. In a comprehensive study of calibration standards Earp *et al.* [28] tested several fluorescent dyes and concluded that fluorescein Sodium Salt is the most suitable fluorescent standard for instrument performance checks and calibration of chlorophyll *a* fluorometers. The excitation and emission spectra of chlorophyll *a* [18], [20], [29]–[33] and the fluorescence simulant fluorescein (Sigma-Aldrich) [28], [34] are shown in Fig. 1.

As explained earlier, due to the low concentration of fluorophores in water the fluorescence emission is significantly lower than the excitation light. Therefore, excitation light and emission filters play critical role in the system. It is very important for the excitation light to overlap as much as possible with the excitation spectrum of the target fluorophore, in order to gain maximum fluorescent signal. Additionally the emission filter must provide sufficient attenuation to ensure that the signal received by the sensor is the emission light.

Two light emitting diodes (LEDs) have been selected as potential candidates for fluorescein excitation source LED405E (Thorlabs) and LED465E (Thorlabs). For the emission filter, we have chosen to manufacture absorption filters rather than dichroic filters. Though it has been demonstrated that dichroic filters could act as an emission filter in contact fluorescence imaging systems

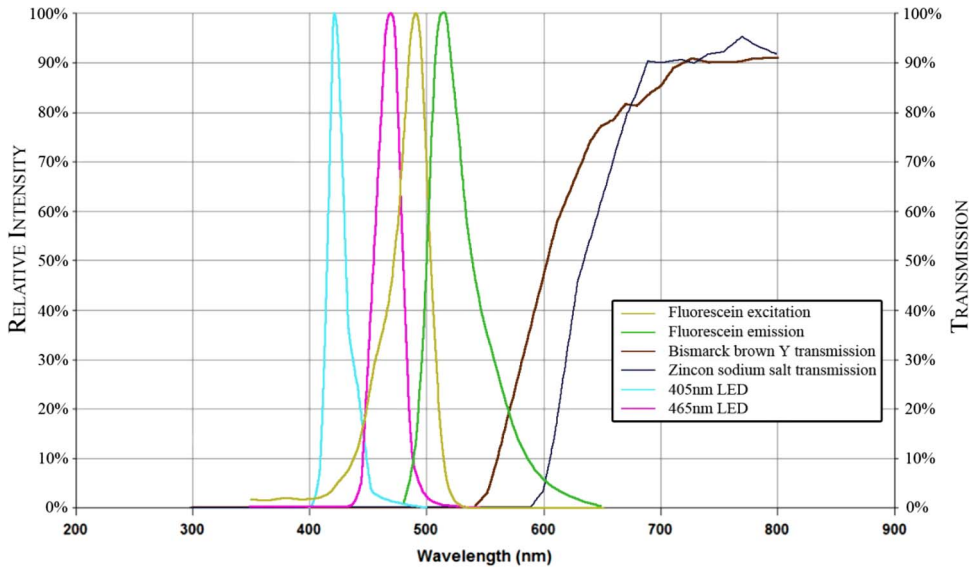

Fig. 2. Excitation spectra of fluorescein, emission spectra of LED405E and LED465E, and transmission spectra of BBY and ZSS. From the overlaid spectra, we can conclude that the combination of LED465E as the excitation source with BBY as the emission filter would be most efficient provided that leakage of excitation light does not occur.

[35], they have several disadvantages. Dichroic filters are dependent on the angle of incident light (unlike absorption filters), they have complex design, and are expensive and complicated to manufacture (due to the multiple layers) [15], [36]. Bismarck brown Y (Sigma Aldrich) and Zincon sodium salt hydrate (Sigma Aldrich) were selected as potential candidates for absorbing dye in the emission filter for fluorescein. The excitation and emission spectra of fluorescein, emission spectra of LED405E and LED4065E; transmission of Bismarck brown Y (BBY) and Zincon sodium salt hydrate (ZSS) are shown in Fig. 2. From the overlaid spectra we observe that LED465E has more overlay with the excitation spectrum of fluorescein when compared to LED 405E. Also, BBY transmits more of the emission light from fluorescein when compared to ZSS. Therefore, the combination of LED465E as excitation source with BBY as emission filter would be most efficient providing that leakage of excitation light does not occur.

Excitation light and emission filter compatibility together with filter thickness optimization were tested empirically. For the purpose of testing, the necessary thickness for optical density (OD) 4, 5 and 6 was calculated for both BBY and ZSS. The calculations were done by using Beer–Lambert law, Eq. (1), where I and I_0 are the intensity of the transmitted and incident light accordingly (I/I_0 is the optical density), ε is the extinction coefficient, l is the absorption filter thickness and c is the concentration of the absorption dye in the filter.

$$\frac{I}{I_0} = 10^{-\varepsilon l c} \tag{1}$$

For both absorption dyes we have used the solubility limit as the concentration to keep the filter thickness to a minimum (to keep the light collection efficiency to a maximum). For BBY $\varepsilon = 32\,000$ L/(mol $\cdot$ cm) [37], the dye content is 50% and $c = 11$ g/l, yields $l = 95$ μm, 119 μm and 143 μm for OD 4, 5 and 6 accordingly. For ZSS $\varepsilon = 10\,000$ L/(mol $\cdot$ cm) [38], and $c = 10$ g/l, yields $l = 185$ μm, 231 μm, and 277 μm for OD 4, 5, and 6 accordingly. Polyvinyl acetate (Sigma-Aldrich) was chosen as a polymer to be loaded with the absorption dye. We have chosen Polyvinyl acetate for its optically transparent, inexpensive and biocompatible properties [15]. To manufacture the filter, Polyvinyl acetate was dissolved in methanol and the desired absorption dye (BBY or ZSS) was added in the required concentration. By using spin coating technique the solution was applied

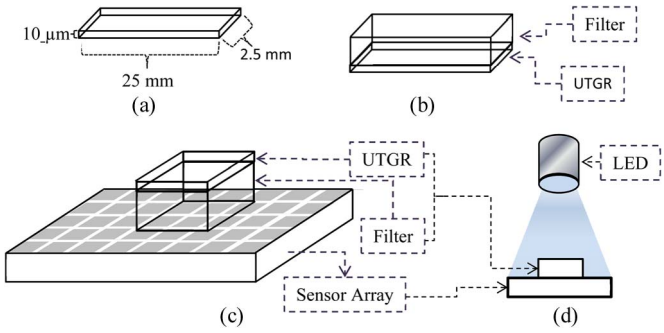

Fig. 3. (a) Schematic of the ultra-thin glass strip used as a substrate for spin coating, (b) manufactured filter on top of the glass strip, and (c) manufactured filter of top of UTGR attached to a CIS pixel array. (d) Simplified schematic of the system used to test filter's ability to attenuate excitation light.

to an UTGR (Nippon Electric Glass), and allowed to dry for 24 hours. The UTGR is 10 μm thick and 2.5 mm wide strip, the length can be several meters long; we have cut it to 25 mm strips. It is flat therefore making it a great fit for spin coating substrate. The small thickness of the UTGR minimizes its impact on the light collection efficiency of the contact fluorescence system. It is transparent in the visible region, and therefore does not modulate the optical properties of the filter. Additionally, the UTGR can be cut to desired size after the filter has been applied. This allows us to shape and size the filter to fit the whole or a part of the CIS's array. To apply the filter to the CIS array we have flipped the filter glass side up and attached it to the sensor array using small amount of PVAc solution as an adhesive. A schematic (not to scale) of UTGR, a manufactured filter on top of UTGR and attached to a sensor array is shown in Fig. 3.

For the purpose of testing the manufactured filters for light leakage and selecting the optimal emission filter (in terms of thickness and absorption dye), the different available filters were applied one at a time to the sensor array. A schematic of the system used is presented in Fig. 3(d). For each filter applied, the following images were captured from the sensor: reference (darkness), LED405E on and LED465 on. During all the experiments parameters that affect the image such as integration time, offset, and gain were kept constant. The acquired images have been processed and the signal pixels have been segmented. The image segmentation is done by using signal uniformity and performing region growth within the filter area; 100 pixels from the center of the filter are sampled for initial signal. The following algorithm is run by iterations, mean value of the signal is calculated, and area growth is performed with the criteria of 1% tolerance from the calculated mean value. When the growth reaches 0 pixels per iteration the pixels are considered to be segmented. The rest of the pixels are either affected by leakage light or not covered by the filter at all. A sample image captured by the sensor from LED465E excitation with Bismarck brown Y filter attached is shown in Fig. 4. It can be seen that the filter is not aligned (horizontally or vertically). However, using the method described above for pixel selection, allows us to choose the desired pixels and only the desired pixels, as long as they are grouped together regardless of the shape or alignment of the filter. In Fig. 4 the pixels that were classified as signal are bound by the red line. Though the selected area may seem small, it consists of over 67 000 pixels. To quantify the filters attenuation, the mean gray value (MGV) of the pixels within the red line was calculated via equation (2). In the equation, A_{filter} is the area within the red line $I(x, y)$ is the gray level of a pixel at coordinates (x, y). The gray level of a single pixels is measured by digital numbers (DNs). Digital number is an integer that varies between 0 to 255, where 0 is a complete darkness and 255 is at saturation. The MGV however does not have to be zero because it is an average; the lower the MGV is the better the filter attenuates the excitation light

$$\langle I \rangle = \frac{\sum_{(x,y)\in A_{\text{filter}}} I(x, y)}{A_{\text{filter}}}. \tag{2}$$

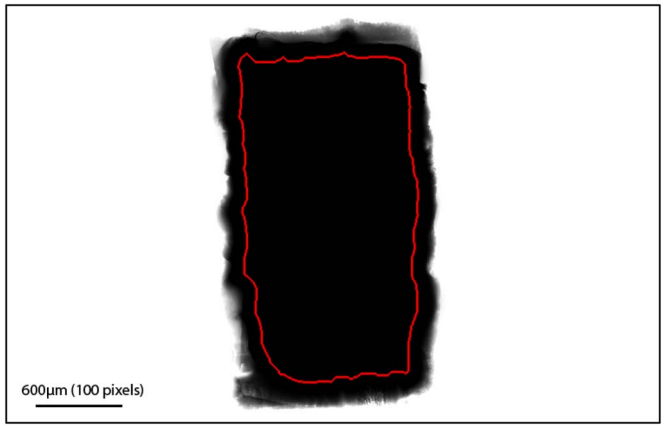

Fig. 4. Sample image of a Bismarck brown Y filter attached to the sensor array. LED465E is on, LED405E is off. The pixels within the red line are the signal (segmented iteratively by applying area growth starting with 100 pixels from the center). Mean gray value of the pixels within the red line is calculated and used for comparison of leakage light.

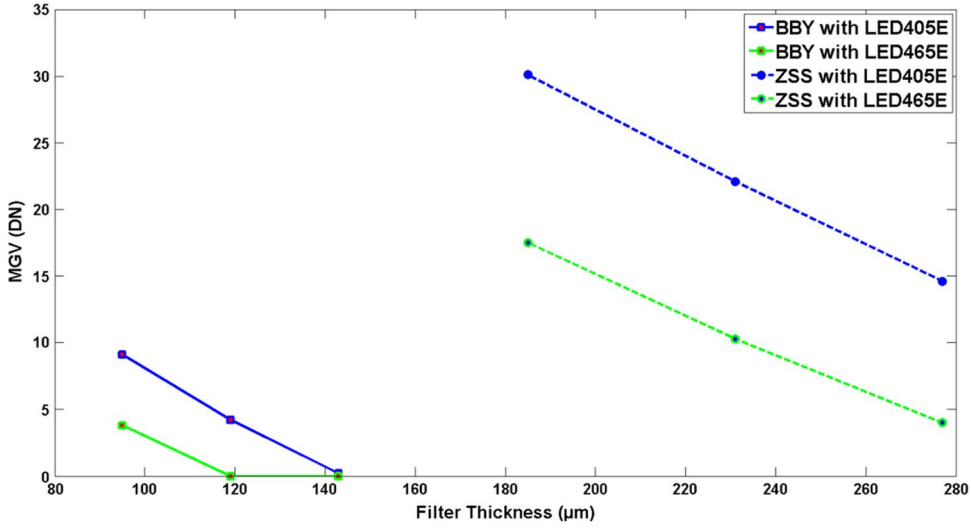

Fig. 5. Measured MGVs acquired from different combinations of filter thickness, absorption dye, and excitation source. ZSS has showed leakage light for both excitation sources and has been empirically established to be unfit as an absorption dye. BBY has shown good attenuation of LED405 at filter thickness 143 μm and even better attenuation of LED465E at filter thickness 119 μm and above.

Signals captured with ZSS filters showed leakage light for both LED405E and LED465E, for all filters thicknesses. BBY filters have performed well in combination with LED465E at thicknesses of 119 μm and 143 μm, BBY showed very weak leakage light with LED405E at 143 μm. The calculated MGVs are presented in Fig. 5. Based on the acquired results we have chosen the 119 μm thick PVAcBBY filter with the combination of LED465E as the optimal combination for maximum transmission of fluorescence emission and good attenuation of the excitation light.

3. Excitation Source and Emission Filter for Lensless Miniature Portable Fluorometer for Measurement of CDOM in Water

Unlike chlorophyll *a*, CDOM is not a single molecule. Rather it is a collection of different matter with similar properties, making the excitation spectra of CDOM broad with multiple excitation and emission peaks. While the excitation spectrum is mostly between 300 nm to 400 nm, the emission

TABLE 1

Description, excitation, and emission spectra of CDOM, from Coble *et al.* [39], [40]

Description	Excitation Peak (nm)	Emission Peak (nm)
UV-humic	<260	400-460
Visible -humic	320-360	420-460
Marine-humic	290-310	370-410
Protein-like	275	305-340

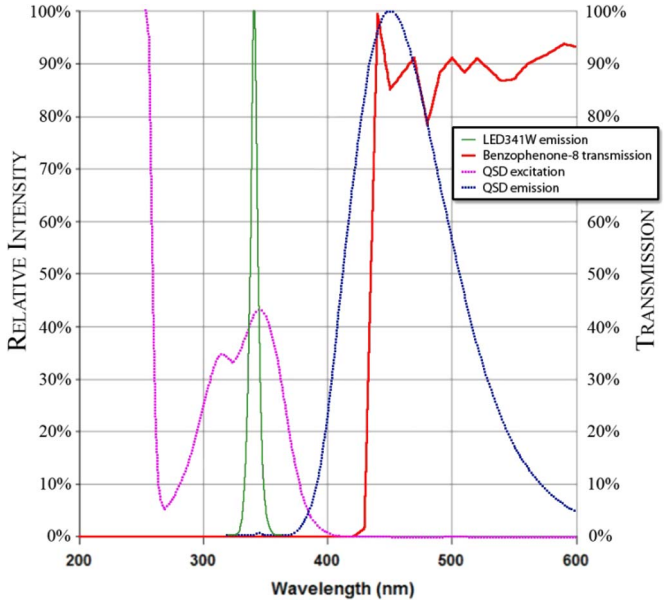

Fig. 6. LED341W emission spectrum (used for fluorescence excitation), Benzophenone-8 transmission spectrum, and QSD excitation and emission spectra.

spectrum is between 400 nm to 500 nm. Coble *et al.* [39], [40] proposed a classification of CDOM based on its origin, Table 1.

Quinine Sulfate Dihydrate (QSD) is a calibration standard [41] for fluorometers. Moreover, it is used as a standard unit to measure CDOM concentration in water [21], [28], [42]–[47]. One quinine sulfate dehydrate Unit (QSU) $=$ 1 μg quinine sulfate/L $=$ 1 ppb $=$ 1.28 nM [42], [48]. In this paper, we measure fluorescence directly from QSD and report our results in QSU. LED341W has been selected as an excitation source for QSD. We have selected this LED because of the proximity of the peak emission of the LED at 341 nm and the peak excitation of QSU at 347 nm. Benzophenone-8 was chosen as the absorbing dye for the emission filter of QSD, based on previously reported work [15], [36] where Blockstein *et al.* reported PVAcB-8 filter that was tested and proven to be efficient at attenuating 340 nm (and 380 nm) excitation light. For the filter manufacturing PVAc was dissolved in Methanol and Benzophenone-8 was added to a concentration of 100 g/l. The solution was spin coated on top of UTGR to manufacture 20 μm thick layer. The excitation spectrum of LED341W is shown in Fig. 6 together with the absorption spectrum of Benzophenone-8 and the excitation and emission spectra of QSD.

4. Integrated Fluorometer System

The combined system is a portable miniature lensless fluorometer designed to measure two different fluorophores. For the excitation light two LEDs were previously chosen; LED465E for fluorescein and LED 341W for quinine. The CIS used in the system is Aptina MT9V032; this CIS has been chosen due to its low light detection ability (sub 0.1 lx) and monochrome design. No Bayer

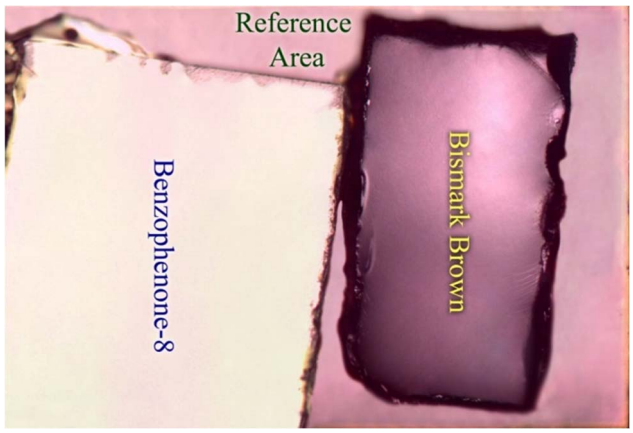

Fig. 7. Image of the sensor array with PVAcBBY and PVAcB-8 filters attached to it. Though the filters have different shapes both in terms of size and alignment by using the simple pixel sorting technique, we are able to sort out the signal pixels.

filter allows us to fully control the wavelengths reaching the pixels by attaching our filter on top of the sensor array. The CIS mounted on a FPGA board (part number UI-1222LE-M-GL) was purchased from 1stVision Inc. The size of the FPGA board is $36 \times 36 \times 8$ mm $(\mathrm{H} \times \mathrm{W} \times \mathrm{D})$. The sensor package is a sealed package with a glass lid (borosilicate glass) cover above the sensor which protects the sensor from external hazards and prevents contact [49]. The borosilicate glass was removed to gain access to the CIS pixel array [36]. The MT9V032 is packaged in a standard wire bonding package; a common method for bonding the sensor die to the packaging, it utilizes micro-wires that are 30 microns in diameter and can be easily severed. In order to protect the bond wires, they were covered with M-COAT C air drying silicone rubber (InterTechnology Inc.). The silicone rubber was applied to the wire bonding area and allowed to dry for a period of 24 hours [36]. Upon drying, the silicone rubber hardens and creates a protective shell [50], [51]. Protecting the wire bonds allows us to safely attach an emission filter on top of the sensor array. By separating a single CIS into two parts, the system uses pixel array of a single CIS to measure fluorescence from two different fluorophores. Two absorption filters are used for attenuation of the excitation light (originated by the LEDs). The filters are manufactured separately by using the manufacturing method and specifications previously mentioned. When ready, the filters are attached to the sensor array. Though this is a very crude method of applying multiple emission filters on top of a sensor array, it has several advantages. First, it is very simple, both in terms filters fabrication method and attaching them to the sensor array. Second, it allows us to easily remove the attached filters. Finally, it allows us to attach two filters with very different thickness to the filter array. Fig. 7 is a typical microscope image of two different emission filters attached to a single sensor array. The attached filters are not aligned and have different size and tilt. However, by using simple pixel segmentation technique previously presented, we can easily segment the pixels that carry the signal regardless of size or shape of the filter. The schematic of the integrated fluorometer is shown in Fig. 8.

The system has been waterproofed by sealing the electric components via liquid silicone. The silicone was applied around exposed wires and allowed to dry for a period of 24 H. Upon drying, the system was submerged in a body of water (fish tank), tested and found to be operational while submerged. Several pictures of the system while submerged and working were captured by camera. Fig. 9(a) shows a close up of the system while operating. We have chosen to keep LED465E on to show that the system is operational, we could not capture LED341W because it emits UV light that we cannot see by eye or capture on camera. Fig. 9(b) shows the system with the body of water with the laptop connected to the system. We have moved the battery in this picture to show that the system is not limited to a specific configuration. The received signal was in saturation (as can be seen in the image) because of the white light component in the room needed for the photography.

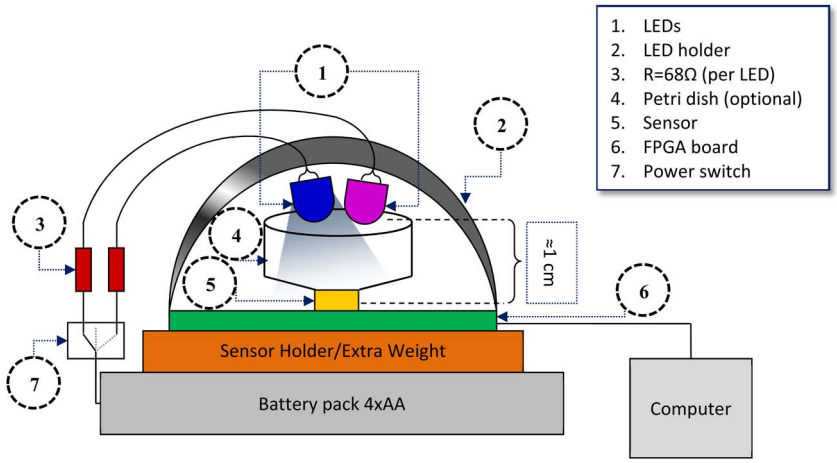

Fig. 8. The schematic of the miniature portable lensless fluorometer. Though not indicated in the figure, the emission filters are attached to the sensor array.

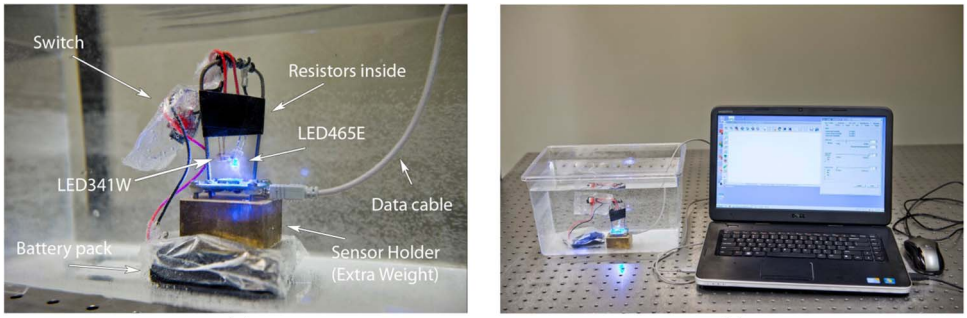

Fig. 9. (a) The system with the Petri dish detached in a close up and (b)the system while operating within the body of water connected to a laptop.

The power consumption of the system was calculated to be $<$ 340 mW [49], [52], [53] (includes sensor power and excitation light power) when operating at 30FPS and $<$ 120 μW when standby. The prototype system price is $<$ \$500 where the main contributors to the price are the sensor with the FPGA board and the LEDs. The size of the system is 7.6 cm by 7.6 cm by 12.7 cm $(\mathrm{L} \times \mathrm{W} \times \mathrm{H})$, the length and the width are limited by the size of the battery pack and can be further reduced by using a more compact 6 V DC power source. The height can be further reduced by using a different type of LED packaging and by attaching the board directly to the battery, i.e., using the battery as a holder/extra weight for the FPGA board.

5. Fluorometer Calibration and Detection Limit, Results, and Discussion

Following the initial tests of the fluorometer's capability to operate under water, we calibrated the fluorometer. The calibration was performed by measuring the fluorometer's response to different concentrations of QSD and fluorescein. For the purpose of this experiment, we have chosen not to submerge the complete system in a body of water. Instead, we have attached a Petri dish to the sensor. Attaching a Petri dish allows us to apply smaller amounts of QSD and fluorescein solutions directly between the sensor and the excitation source. Solutions of different concentrations of QSD and fluorescein in water were prepared prior to the experiment. The solutions were stored in small containers; the containers were wrapped in foil to protect them from light (to prevent bleaching). For QSD we have decided to initially prepare the concentrations in QSU units (ppb), because other available devices use ppb, however to report our work in a more cohesive way the concentration

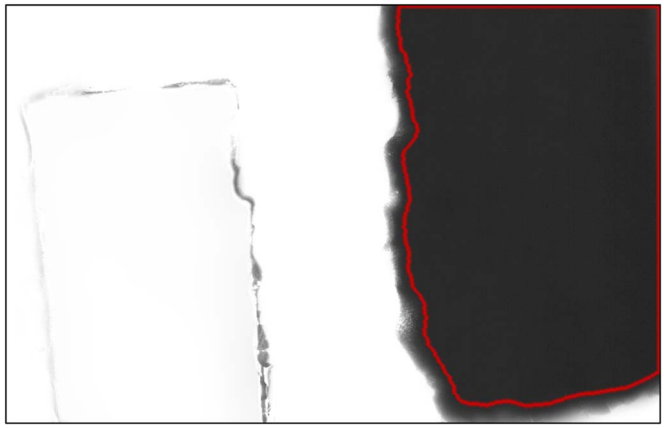

Fig. 10. Fluorescent image of 1.3 nM fluorescein excited with LED465E imaged with an imager that has two filters attached. The filter on the right is PVAcBBY, the pixels within the red line are the signal. The filter on the left is PVAcB-8.

units have been later converted to mol/L. The following concentrations were prepared and measured 1 ppb to 9 ppb in steps of 1 ppb (1.28 nM to 11.5 nM in steps of 1.28 nM), 10 ppb to 90 ppb in steps of 10 ppb (12.8 nM to 115 nM in steps of 12.8 nM), 100 ppb to 500 ppb in steps of 100 ppb (128 nM to 638 nM in steps of 128 nM). For fluorescein the following concentrations were prepared and measured 0.5 nM to 1.5 nM in steps of 0.2 nM, 3 nM to 7 nM in steps of 1 nM, 10 nM to 70 nM in steps of 10 nM, 100 nM to 400 nM in steps of 100 nM and 1000 nM. The following integration times were used for measuring fluorescence from both QSD and fluorescein 5 ms, 10 ms, 20 ms, 40 ms, 60 ms, 80 ms, 100 ms, 140 ms, 180 ms, 250 ms, 500 ms, 750 ms, and 1000 ms. After collecting all the data for the different concentrations for the different filters and different integration times, the images were processed. The same pixel sorting method previously used was applied, a group of 100 pixels from the center of the relevant filter are sampled for initial signal and area growth was performed by iterations until all the relevant neighbor pixels were selected. For the selected pixels, we calculated MGV while the information from the rest of the pixels was ignored (rest of the pixels either do not have any filter attached or have another filter attached and therefore are irrelevant). Fig. 10 shows sample fluorescent image acquired from our system with two filters attached, the left filter is PVAcB-8 and the right filter is PVAcBBY. The excitation source is LED465E, the integration time is 1000 ms, and the water is loaded with fluorescein with 1.3 nM concentration. The pixels within the red area are the signal. It can be seen that the area under the PVAcB-8 is saturated because the filter transmits the excitation light produced by LED465E. The edges have increased light attenuation due to additional reflection and hence imaged as darker silhouette.

After acquiring and analyzing the results, we have chosen three different integration times for fluorescein fluorescent signal based on two criteria, first criteria is smallest overlap between the signals and second criteria is that the signals must allow us to measure all measurable concentrations. The results are presented in Fig. 11(a). By using similar criteria, we have chosen two integration times for QSD fluorescent signal. The results are presented in Fig. 11(b). Fluorescein measurement requires three different integration times (while QSD requires only two) because of the larger concentration range measured. Fluorescein concentration range is $1000\ \text{nM}/0.7\ \text{nM} = 1429$, while the QSD concentration range is $638\ \text{nM}/2.55\ \text{nM} = 250$. For fluorescein, a 1000 ms integration time covers concentration range between 0.7 nM to 10 nM, 180 ms integration time covers concentration range between 3 nM to 60 nM and 10 ms integration time covers 30 nM to 1000 nM. For QSD, 1000 ms integration time covers concentration from 2.55 nM to 51 nM and 80 ms integration time covers the concentration from 25.5 nM to 638 nM.

For measuring the confidence interval of our results, uniform light was projected on the sensor and a signal was captured at different integration times. The signals from the pixels were analyzed by fitting the signal distribution to Gaussian in order to find the standard deviation. The confidence

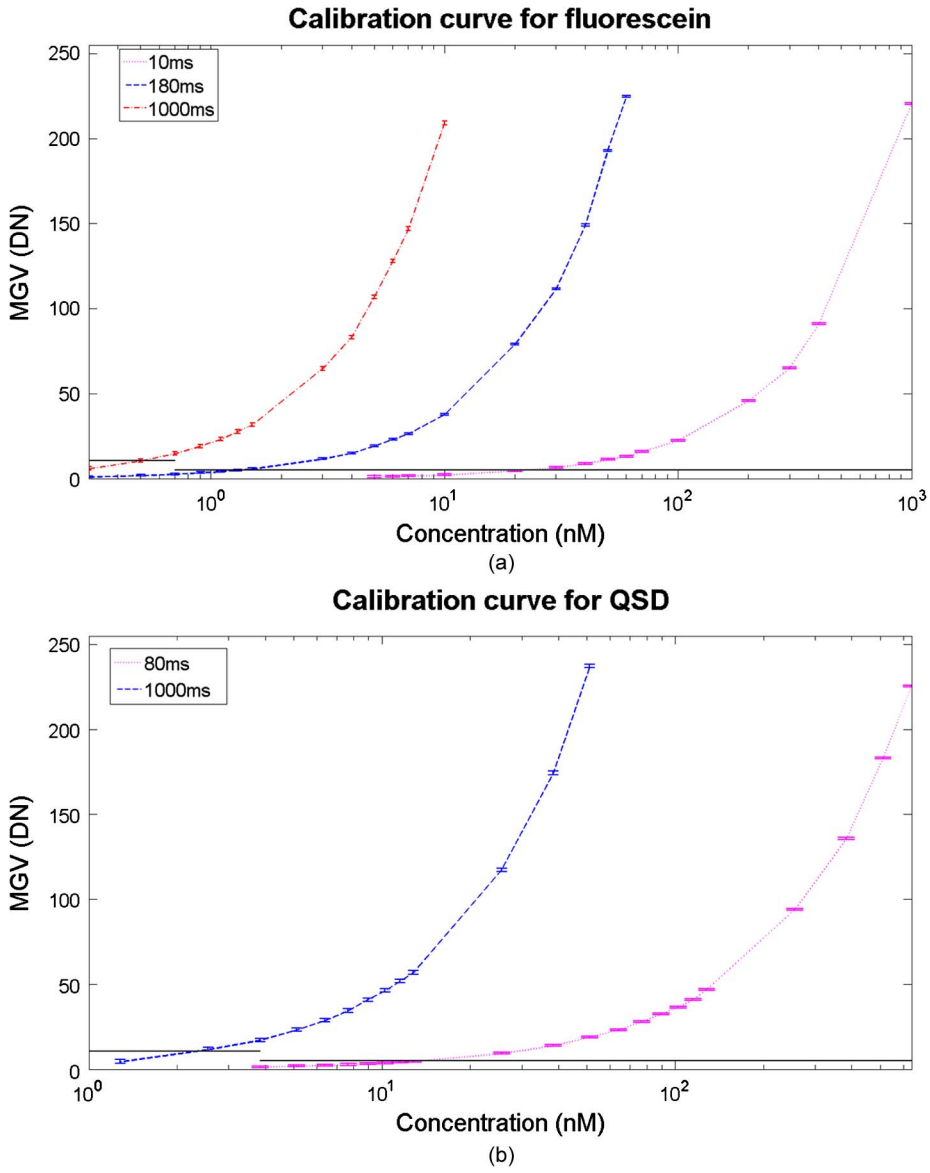

Fig. 11. (a) Fluorescent signal acquired from fluorescein at 10 ms, 180 ms, and 1000 ms integration time as a function of different concentrations. (b) Fluorescent signal acquired from QSD at 80 ms and 1000 ms integration time as a function of different concentrations. The horizontal lines show SNR = 10 threshold.

interval was set to 95% (two times standard deviation). The calculated confidence interval for integration times 10 ms, 80 ms and 180 ms was less than 0.5 DN. However, the error of any electronic device is half of the last precision number, therefore the confidence interval for those integration times have been set to 0.5 DN. For 1000 ms integration time, the confidence interval was calculated to be 1 DN. From the acquired confidence intervals, using signal to noise ratio (SNR) of 10 as a signal detection threshold, we have calculated that the systems detection limit is 5 DN, 5 DN, 5 DN and 10 DN for 10 ms, 80 ms, 180 ms and 1000 ms integration time accordingly. By applying the known signal detection limit the detection limit for fluorescein is 0.7 nM at integration time 1000 ms and the detection limit for QSD is 2.55 nM also at integration time 1000 ms.

We could increase integration time further to try and measure smaller concentrations of both fluorescein and QSD. However, we have chosen not to do so for two main reasons. First, increasing

TABLE 2

A comparison between our system to other systems for benchmark purposes

	Commercial			Prototype			
	WET Labs ECO Triplet	Turner Designs C3	YSI 6600 V2	A	B	C	D
QSD detection	V	V	V	X	X	X	V
Limit of detection	0.12 nM	0.19 nM	0.5 nM	----	----	----	2.55 nM
Dynamic range	5556	33333	6250	----	----	----	1000
Fluorescein detection	V	V	V	V	V	V	V
Limit of detection	0.022 nM	0.028 nM	0.11 nM	3.5 μM	340 nM	0.4 nM	0.7 nM
Dynamic range	6222	20000	4000	----	----	----	1428
Power Consumption	350 mW to 750 mW	<2400 mW	----	----	----	----	340 mW
System Size	6.3 cm x 12.3 cm (DxL)	10 cm x 23 cm (DxL)	8.9 cm x 49.8 cm (DxL)	----	----	----	7.6cmx7.6cmx12.7cm (LxWxH)
System Cost	>$10,000	>$8000	>$10,000	<$1000	----	----	<$500

integration time increases the amount of power required by the system for a single measurement. Second, large integration times increase noise. This increases the confidence interval (which decreases result's reliability) and causes increase in the SNR $= 10$ threshold (which reduces the active dynamic range).

In order to benchmark our results we have compared our system to other recently reported miniature fluorometers designed for remote sensing of chlorophyll concentration in water. Unfortunately we have not been able to find similar systems for measuring CDOM. The systems used for comparison are labeled as system A [18], B [11], C [20] and D (our system), unfortunately information such as power consumption, system size and cost are rarely reported. Additionally we have compared our system to several commercial water quality systems, the systems are labeled as WET Labs ECO FL [54], Turner Designs C3 [55] and YSI 6600 V2 [56], [57]. The data is presented in Table 2.

The typical chlorophyll *a* values for surface water are 0.5–340 nM [58]–[60]. It is more difficult to report the typical values of CDOM concentration in surface water because of less available research. Based on multiple data sources that we are aware of we can report that the typical CDOM values are between 0.64 nM to 290 nM [5], [21], [42], [46], [47], [61], [62]. Though our prototype system is capable of detecting lower concentrations of chlorophyll *a* than some other systems (specifically A and B), further increase in sensitivity is required to detect the lower end concentrations typically seen for chlorophyll *a* and CDOM. Increased sensitivity can be achieved by either increasing the intensity of the excitation light or by increasing the light sensitivity of the sensor. Increase of excitation light output requires higher power LEDs with higher power consumption. Increase in light sensitivity requires improved CMOS imager sensor with lower detection limit; newer and improved CISs may also decrease the power consumption. However, it will cause a sharp increase in price ($2000 and up). For the current prototype, we have decided to prove the concept by using previously proven sensor [15], [36]. It is important to note that the prototype system offers a wide range of concentration measurements for both CDOM and chlorophyll; additionally it covers most of the typical concentrations for both fluorophores in surface water. Our prototype system has a relatively small volume 737 cm^3, can be compared to 383 cm^3, 1806 cm^3, and 3098 cm^3 for ECO FL, C3 and 6600 V2 accordingly. Our system is the most cost effective when compared to all other systems and as far as the authors are aware, the only reported proof-of-concept system that offers integrated fluorometer for two fluorophores via a single sensor array. Finally, our system offers the lowest power consumption when compared to other systems with known power consumption.

6. Conclusion

In summary, here we demonstrate a proof of concept of a lensless miniature portable fluorometer for measurement of chlorophyll and CDOM in water. The system is waterproof and has been demonstrated to operate while submerged under water. The system utilizes two LEDs for excitation light LED341W and LED365E. The system is capable of performing fluorescence imaging of two different fluorophores by using a single sensor array. Two filters are attached to the sensor array for excitation light attenuation, PVAcBBY and PVAcB-8. As far as the authors are aware this is the first time that a miniature fluorescence contact imaging system using a single CIS pixel array to measure fluorescent signal from two different fluorophores is demonstrated. The system has been tested with fluorescein to simulate chlorophyll *a* and has showed the ability to successfully resolve signal for concentrations between 0.7 nM to 1000 nM. The system has been tested with QSD and was shown to successfully resolve signal for concentration between 2.55 nM to 638 nM.

The cost of the system has been calculated to be under $500, where most of the expenses are for the CIS with the FPGA board and the LEDs. This is significantly lower than other systems with known cost. The power consumption of the system was calculated to be under 340 mW when operating at 30 FPS and under 120 μW when in standby mode. This is lower than other systems with known power consumption. The size of the system is 7.6 cm $\times$ 7.6 cm $\times$ 12.7 cm (L $\times$ W $\times$ H). However, it can be reduced by removing the FPGA board holder and attaching the FPGA board directly to the power source. The size can be additionally reduced by choosing more compact power source and LEDs.

These results shows that using a single CIS pixel array for integration of more than one contact fluorescence system is achievable and an effective alternative to module based equipment that consists of a platform with multiple detachable modules where each module measures single parameter. The filter application method used in this work lacks high precision, but it is cost effective. Additionally, it does not require expensive equipment (that is required for lithography), easy to implement and proven to be efficient. Future development of this technology is most likely to include more integration for more fluorescent applications and will require improved filter integration such as achieved by lithography. However, we consider the reported system as an important milestone towards the future work and for this purpose, we found the reported filter application technique to be adequate.

Due to the properties of the UTGR it has no considerate impact on filter thickness (which affect light collection efficiency) or the optical transmission/absorption properties of the filter. It is easy to handle and can be used as a substrate for lithography (similar to silicon wafer). In future work, more filters in small area can be manufactured in groups on top of UTGR substrate (using lithography) and attached to a CIS pixel array as a premade group. This integration will allow expanding the usability of a single sensor to measure more parameters. Examples of other parameters that can be optically measured are turbidity, Uranine, Phycoerythrin, Phycocyanin, Oil, Tryptophan and others. Future devices may contain spatially smaller filters limited to a size of 100 by 100 pixels (600 μm by 600 μm). For the current sensor this will allow to hold as many as 28 various filters while leaving some of pixels to be reference pixels.

Shaping excitation spectrum can be done only by starting with wideband light source. Spectrum shaping is done by attenuating the undesired wavelengths while keeping the ones required for excitation. This approach is vastly used in the conventional optical devices. Typically a mercury-xenon lamp is used because it produces wavelengths starting from 200 nm and up (to beyond 1000 nm). The produced light is being filtered by band pass filter to choose specific wavelength that is required for excitation. Subsequently this is a very power inefficient system. A portable miniature system cannot use this kind of mechanism, because it is imperative to preserve power in order to prolong the longevity of the system. Therefore, we have used two LEDs, where each LED was designated for excitation of specific fluorophore. We expect that in the future the amount of the excitation sources will grow together with the amount of filters. Compact LED packaging will be required for high LED integration into a small area.

Additional improvement in the concentration detection limited relies on the ability of the system to detect low light signal. The CIS used in this paper is rated as under 0.1 lx, however newer and more sensitive CISs exist that are capable to detect 0.01 and even 0.001 lx. We have decided not to include those sensors in our prototype because of the price (that can reach over $5000). However, in the future the price will drop and thus by using this technology it will be possible to create cheap, compact integrated systems with lower detection limit.

Acknowledgment

The authors acknowledge Dr. C. Dalton and Dr. C. Hayden, AMIF Laboratory, University of Calgary, for their help and support in cleanroom with manufacturing of our PVAcB-8 and PVAcBBY filter. We acknowledge Dr. R. J. Turner for access to the spectrometer equipment funded by NSERC, CIHR, and AHFMR. We acknowledge P. Mintchev for his help and support when using the spectrometer and a spin coater. We thank F. Hickley, C. Simon, and W. Flaman for their contribution and assistance in technical issues.

References

[1] M. Chen *et al.,* "A red-shifted chlorophyll," *Science*, vol. 329, no. 5997, pp. 1318–1319, Sep. 2010.
[2] R. E. Blankenship, N. Scales, Y. Li, M. Chen, and R. D. Willows, "Extinction coefficient for red-shifted chlorophylls: Chlorophyll D and chlorophyll f," *Biochim. Biophys. Acta, Bioenerg.*, vol. 1817, no. 8, pp. 1292–1298, Aug. 2012.
[3] D. A. Hansell and C. A. Carlson, *Biogeochemistry of Marine Dissolved Organic Matter*. San Diego, CA, USA: Academic, 2002, p. 774.
[4] C. A. Corbett, "Colored Dissolved Organic Matter (CDOM) workshop summary," Univ. South Florida, Tampa, FL, USA, 2007.
[5] J. Para *et al.,* "Fluorescence and absorption properties of Chromophoric Dissolved Organic Matter (CDOM) in coastal surface waters of the Northwestern Mediterranean Sea, influence of the Rhône River," *Biogeosciences*, vol. 7, no. 12, pp. 4083–4103, Dec. 2010.
[6] B. D. Downing *et al.,* "Quantifying fluxes and characterizing compositional changes of dissolved organic matter in aquatic systems *in situ* using combined acoustic and optical measurements," *Limnol. Oceanogr. Methods*, vol. 7, pp. 119–131, Jan. 2009.
[7] Y. Zhang *et al.,* "Characteristics and sources of chromophoric dissolved organic matter in lakes of the Yungui Plateau, China, differing in trophic state and altitude," *Limnol. Oceanogr.*, vol. 55, no. 6, pp. 2645–2659, Nov. 2010.
[8] J. F. Saraceno *et al.,* "High-frequency *in situ* optical measurements during a storm event: Assessing relationships between dissolved organic matter, sediment concentrations, hydrologic processes," *J. Geophys. Res.*, vol. 114, no. G4, pp. G00F09-1–G00F09-11, Dec. 2009.
[9] R. Pienitz and W. F. Vincent, "Effect of climate change relative to ozone depletion on UV exposure in Subarctic Lakes," *Nature*, vol. 404, no. 6777, pp. 484–487, Mar. 2000.
[10] J. Bunt, "Light and photosynthesis in aquatic ecosystems," *Aquat. Bot.*, vol. 50, no. 1, pp. 111–112, Apr. 1995.
[11] T. D. James *et al.,* "Valve controlled fluorescence detection system for remote sensing applications," *Microfluid. Nanofluid.*, vol. 11, no. 5, pp. 529–536, Nov. 2011.
[12] C. Cheng, Y. Wei, X. Sun, and Y. Zhou, "Estimation of chlorophyll-a concentration in turbid lake using spectral smoothing and derivative analysis," *Int. J. Environ. Res. Public Health*, vol. 10, no. 7, pp. 2979–2994, Jul. 2013.
[13] O. Holm-Hansena *et al.,* "Temporal and spatial distribution of chlorophyll-a in surface waters of the Scotia Sea as determined by both shipboard measurements and satellite data," *Deep. Sea Res. II, Top. Stud. Oceanogr.*, vol. 51, no. 12/13, pp. 1323–1331, Jun. 2004.
[14] S. Jamshidi and N. Bin Abu Bakar, "A study on distribution of chlorophyll-〈I〉a〈/I〉 in the coastal waters of Anzali Port, South Caspian Sea," *Ocean Sci. Discuss.*, vol. 8, no. 1, pp. 435–451, Feb. 2011.
[15] L. Blockstein, C. C. Luk, A. K. Mudraboyina, N. I. Syed, and O. Yadid-Pecht, "A PVAc-based benzophenone-8 filter as an alternative to commercially available dichroic filters for monitoring calcium activity in live neurons via Fura-2 AM," *IEEE Photon. J.*, vol. 4, no. 3, pp. 1004–1012, Jun. 2012.
[16] J. Reichman, *Handbook of Optical Filters for Fluorescence Microscopy*. Bellows Falls, VT, USA: Chroma Technology Corp., 2010.
[17] M. Sauer, H. Johan, and E. Jörg, *Handbook of Fluorescence Spectroscopy and Imaging: From Ensemble to Single Molecules*. Weinheim, Germany: Wiley-VCH, 2010.
[18] J. Kissinger and D. Wilson, "Portable fluorescence lifetime detection for chlorophyll analysis in marine environments," *IEEE Sensors J.*, vol. 11, no. 2, pp. 288–295, Feb. 2011.
[19] F. Lefèvre *et al.,* "Algal fluorescence sensor integrated into a microfluidic chip for water pollutant detection," *Lab Chip*, vol. 12, no. 4, pp. 787–793, Feb. 2012.
[20] J. J. Lamb, J. J. Eaton-Rye, and M. F. Hohmann-Marriott, "An LED-based fluorometer for chlorophyll quantification in the laboratory and in the field," *Photosynth. Res.*, vol. 114, no. 1, pp. 59–68, Oct. 2012.

[21] G. B. Gardner, R. F. Chen, and A. Berry, "High-resolution measurements of Chromophoric Dissolved Organic Matter (CDOM) in the Neponset River Estuary, Boston Harbor, MA," *Mar. Chem.*, vol. 96, no. 1/2, pp. 137–154, Aug. 2005.
[22] H. Ji, D. Sander, A. Haas, and P. A. Abshire, "Contact imaging: Simulation and experiment," *IEEE Trans. Circuits Syst. I, Reg. Papers*, vol. 54, no. 8, pp. 1698–1710, Aug. 2007.
[23] K. Salama, H. Eltoukhy, A. Hassibi, and A. El-Gamal, "Modeling and simulation of luminescence detection platforms," *Biosens. Bioelectron.*, vol. 19, no. 11, pp. 1377–1386, Jun. 2004.
[24] A. Greenbaum *et al.,* "Imaging without lenses: Achievements and remaining challenges of wide-field on-chip microscopy," *Nat. Methods*, vol. 9, no. 9, pp. 889–895, Sep. 2012.
[25] *Chlorophyll a From Anacystis Nidulans Algae Product Information*, Sigma Aldrich, St. Louis, MO, USA, p. 1.
[26] *Turner Designs Fluorometric Chlorophyll Analysis FAQ*, Turner Designs, Sunnyvale, CA, USA, pp. 1–5.
[27] *Chlorophyll a From Spinach Product Information*, Sigma Aldrich, St. Louis, MO, USA, p. 1.
[28] A. Earp *et al.,* "Review of fluorescent standards for calibration of *in situ* fluorometers: Recommendations applied in coastal and ocean observing programs," *Opt. Exp.*, vol. 19, no. 27, pp. 26 768–26 782, Dec. 2011.
[29] C. S. Yentsch and D. W. Menzel, "A method for the determination of phytoplankton chlorophyll and phaeophytin by fluorescence," *Deep Sea Res. Oceanogr. Abstr.*, vol. 10, no. 3, pp. 221–231, Jul. 1963.
[30] R. Tanaka and A. Tanaka, "Chlorophyll cycle regulates the construction and destruction of the light-harvesting complexes," *Biochim. Biophys. Acta*, vol. 1807, no. 8, pp. 968–976, Aug. 2011.
[31] A. N. Misra, M. Misra, and R. Singh, "Chlorophyll fluorescence in plant biology," in *Biophysics*, P. D. A. N. Misra, Ed. Rijeka, Croatia: InTech, 2012, pp. 171–192.
[32] H. Schubert, U. Schiewer, and E. Tschirner, "Fluorescence characteristics of cyanobacteria (blue-green algae)," *J. Plankton Res.*, vol. 11, no. 2, pp. 353–359, 1989.
[33] P. Held, *Monitoring of Algal Growth Using Their Intrinsic Properties*. Winooski, VT, USA: Biotek, 2011, pp. 1–5.
[34] N. Klonis and W. H. Sawyer, "Spectral properties of the prototropic forms of fluorescein in aqueous solution," *J. Fluoresc.*, vol. 6, no. 3, pp. 147–157, Sep. 1996.
[35] R. R. Singh *et al.,* "A CMOS/thin-film fluorescence contact imaging microsystem for DNA analysis," *IEEE Trans. Circuits Syst. I, Reg. Papers*, vol. 57, no. 5, pp. 1029–1038, May 2010.
[36] A. K. Mudraboyina, L. Blockstein, C. C. Luk, N. I. Syed, and O. Yadid-Pecht, "A novel lensless miniature contact imaging system for monitoring calcium changes in live neurons," *IEEE Photon. J.*, vol. 6, no. 1, pp. 1–15, Feb. 2014.
[37] *Bismarck Brown Y—Product Specification*, Sigma Aldrich, St. Louis, MO, USA, Jan. 8, 2014. [Online]. Available: http://www.sigmaaldrich.com/Graphics/COfAInfo/SigmaSAPQM/SPEC/86/861111/861111-BULK_____SIAL_____.pdf
[38] *Zincon Sodium Salt—Specification Sheet*, Sigma Aldrich, St. Louis, MO, USA, Jan. 8, 2014.
[39] P. G. Coble, "Characterization of marine and terrestrial DOM in seawater using excitation–emission matrix spectroscopy," *Mar. Chem.*, vol. 51, no. 4, pp. 325–346, Jan. 1996.
[40] P. G. Coble, C. E. Del Castillo, and B. Avril, "Distribution and optical properties of CDOM in the Arabian Sea during the 1995 Southwest Monsoon," *Deep Sea Res. II, Top. Stud. Oceanogr.*, vol. 45, no. 10/11, pp. 2195–2223, Aug. 1998.
[41] R. A. Velapoldi and K. D. Mielenz, *A Fluorescence Standard Reference Material: Quinine Sulfate Dihydrate*. Washington, DC, USA: National Measurement Laboratory, National Bureau of Standards, 1980.
[42] C. D. Clarka *et al.,* "CDOM distribution and CO2 production on the Southwest Florida shelf," *Mar. Chem.*, vol. 89, no. 1–4, pp. 145–167, Oct. 2004.
[43] Q. Yu *et al.,* "Functional linear analysis of *in situ* hyperspectral data for assessing CDOM in rivers," *Photogramm. Eng. Remote Sens.*, vol. 76, no. 10, pp. 1147–1158, Oct. 2010.
[44] A. N. Fletcher, "Quinine sulfate as a fluorescence quantum yield standard," *Phorochem. Phorobiol.*, vol. 9, no. 5, pp. 439–444, May 1969.
[45] L. H. H. P. J. S. Robert and J. Kieber, "Photooxidation of triglycerides and fatty acids in seawater: Implication toward the formation of marine humic substances," *Limnol. Oceanogr.*, vol. 42, no. 6, pp. 1454–1462, 1997.
[46] W. Zhu, Q. Yu, Y. Q. Tian, R. F. Chen, and G. B. Gardner, "Estimation of chromophoric dissolved organic matter in the Mississippi and Atchafalaya River plume regions using above-surface hyperspectral remote sensing," *J. Geophys. Res.*, vol. 116, no. C2, pp. C02011-1–C02011-22, Feb. 2011.
[47] A. F. Blumberg, "Distributions of chromophoric dissolved organic matter in New York Harbor," Dept. Civil, Environ. Ocean Eng. Stevens Inst. Technol. Castle Point Hudson, Hoboken, NJ, USA, 2006.
[48] R. N. Conmy, P. G. Coble, and C. E. D. Castillo, "Calibration and performance of a new *in situ* multi-channel fluorometer for measurement of colored dissolved organic matter in the ocean," *Cont. Shelf Res.*, vol. 24, no. 3, pp. 431–442, Feb. 2004.
[49] *1/3-Inch Wide-VGA CMOS Digital Image Sensor*, Aptina, San Jose, CA, USA, 2005, MT9V032 Data Sheet.
[50] M. Beiderman, T. Tam, A. Fish, G. A. Jullien, and O. Yadid-Pecht, "A low-light CMOS contact imager with an emission filter for biosensing applications," *IEEE Trans. Biomed. Circuits Syst.*, vol. 2, no. 3, pp. 193–203, Sep. 2008.
[51] Y. Dattner and O. Yadid-Pecht, "Low light CMOS contact imager with an integrated poly-acrylic emission filter for fluorescence detection," *Sensors*, vol. 10, no. 5, pp. 5014–5027, May 2010.
[52] *LED341W UV LED With Window Specifications and Documentation*, ThorLabs, Newton, NJ, USA, 2011, pp. 1–5.
[53] *LED465E Blue LED Specifications and Documentation*, ThorLabs, Newton, NJ, USA, 2010, pp. 1–5.
[54] *Wet Labs ECO FL*, Wet Labs, Philomath, OR, USA, Jan. 1, 2014. [Online]. Available: http://www.wetlabs.com/eco-fl
[55] *Turner Designs C3 Submersible Fluorometer*, Turner Designs, Sunnyvale, CA, USA, Jan. 18, 2014. [Online]. Available: http://www.turnerdesigns.com/t2/doc/brochures/S-0096.pdf
[56] YSIYSI 6600, 2013, [Accessed: 18-Jan-2014]. [Online]. Available: http://www.ysi.com/media/pdfs/E52-6600V2.pdf
[57] YSIOil in Water Sensor Adapter Kit, Jan. 18, 2014. [Online]. Available: http://www.ysi.com/media/pdfs/E98-Oil-in-Water-Sensor-Adapter.pdf
[58] EOMAP, *Chlorophyll a*, Jan. 19, 2014. [Online]. Available: http://www.eomap.com/chlorophyll

[59] *Chlorophyll a Concentration*, UCL Department of Geography, [Accessed: 19-Jan-2014].
[60] *Trophic State of Alberta Lakes*, Alberta Environment and Sustainable Resource Development, Jan. 19, 2014.
[61] R. F. Chen *et al.,* "Chromophoric Dissolved Organic Matter (CDOM) source characterization in the Louisiana Bight," *Mar. Chem.*, vol. 89, no. 1–4, pp. 257–272, Oct. 2004.
[62] E. Zanardi-Lamardo, C. A. Moore, and R. G. Zika, "Seasonal variation in molecular mass and optical properties of chromophoric dissolved organic material in coastal waters of Southwest Florida," *Mar. Chem.*, vol. 89, no. 1–4, pp. 37–54, Oct. 2004.